

Robust Mars Atmospheric Entry Integrated Navigation based on Parameter Sensitivity

Taishan Lou*

Zhengzhou University of Light Industry, Zhengzhou, 450002, China

Abstract

This paper presented a robust integrated navigation algorithm based on a special robust desensitized extended Kalman filtering with analytical gain (ADEKF) during the Mars atmospheric entry. The robust ADEKF is designed by minimizing a new function penalized by a trace weighted norm of the state error sensitivities and giving a closed-form gain matrix. The uncertainties of the Mars atmospheric density and the lift-to-drag ratio (LDR) percentage are modeled. Sensitivity matrices are defined to character the parameter uncertainties, and corresponding perturbation matrices are proposed to describe the navigation errors respected to the parameter uncertainties. The numerical simulation results show that the robust integrated navigation algorithm based on the robust ADEKF effectively reduces the negative effects of the two parameter uncertainties and has good consistency during the Mars entry.

Keywords: Mars entry; Uncertain parameter; Parameter sensitivity; Desensitized extended Kalman filtering.

1 Introduction

On 6 August 2012, the Curiosity rover of the Mars Science Laboratory successfully landed down at a position approximately 2km from the its target, the Gale Crater, with a touchdown ellipse of $19.1\text{km} \times 6.9\text{km}$ [1]. Although the landing position uncertainties are the smallest in all previous Mars missions, but it is not enough for the future Mars landing exploration missions to have the capability of accurately landing on a high scientific landing site. Factors which contribute to these uncertainties include absence of measurement information, initial entry errors,

* Lecturer, School of Electric and Information Engineering, Zhengzhou University of Light Industry, No.5 Dongfeng Road, Jinshui District; tayzan@sina.com.

atmospheric modeling uncertainties, aerodynamic parameter uncertainties and wind drifts during the entry, descent and landing (EDL) phases [2-4]. New high-precision robust navigation EDL technologies, such as high-precision EDL navigation technology, and autonomous hazard detection and avoidance, are necessary for the future Mars pinpoint landing missions [5-6].

The Mars entry phase is the extremely important and dangerous periods during the EDL phases, and so Mars entry navigation technologies play an important role at a whole precise landing mission [7-8]. However, there is only inertial measurement unit (IMU) is available for entry navigation, because no optical sensors, which are blocked by the vehicle's heat shield and plasma sheath, may be used during the Mars atmospheric entry. Some researchers presented some technologies, such as adaptive sigma point Kalman filter bank, hierarchical mixture of experts' architecture and multiple model adaptive estimation, to reduce the negative effects of the Mars atmospheric density uncertainties, and to attempt to achieve entry navigation precision in the presence of only IMU data [9-11]. However, because of the biases and drifts of IMU, traditional Mars entry vehicles based on IMU dead-reckoning navigation without other external measurement may be lead to larger navigation errors [12-13]. Recent researches show that the Ultra high frequency radio communication was not blocked by the plasma sheath around the entry vehicle, and provides a new integrated navigation scheme that the external measurements will be obtained from the radio communications to improve the online state knowledge during the Mars entry . National Aeronautics and Space Administration (NASA) Mars technology program task is developing an advanced real-time navigation system using the Electra UHF communication between the Mars entry vehicle and an orbiting satellite or a surface beacon, which is preset on the Mars surface or the previous Mars rover of the last mission [16-17]. Levesque and Lafontaine[4] researched four innovative measurement scenarios and their observability based on radio ranging during the Mars atmospheric entry, and augmented some parameters into the navigation state vector by using the Unscented Kalman filter to improve the navigation precision. Li and Peng [18] augmented the constant bias of IMU into the state and addressed the issue of Mars entry navigation using IMU and orbiting/surface radiometric beacons. Li et al. [18] considered large uncertainties in the Martian atmospheric density via a desensitized extended Kalman filter (DEKF). However, for uncertainties of the lift-to-drag ratio (LDR), as a very important aerodynamic parameter of the entry vehicle, only a few literatures play attention on it. Levesque

and Lafontaine [4] analyzed the observability of the LDR, and augmented it into the navigation state vector to estimate. Steinfeldt et al. [20] gives a rule of thumb that increasing L/D by 35% raises chute deployment altitude 1km is given based on experience with EDL simulations. New navigation technologies also must be designed to adaptively or robustly achieve higher navigation accuracy in the LDR uncertainties.

Desensitized optimal control (DOC) methodology, which is originally presented by Seywald and Kumar [21], has been extended and been successfully applied to a wide range of spacecraft optimization problems, such as Mars entry trajectory[22] and Mars pinpoint landing problem of the powered descent phase[23]. The core idea is to embed a penalty function of the sensitivity with a weighting factor into the original performance index and find an optimal compromise between gaining sensitivity reduction and sacrificing the performance. Karlgaard and Shen extended the main characteristic of the DOC methodology to the robust filter design problem such that the performance sensitivity of the filters respected to model uncertain parameters can be reduced[24-25]. The cost function consisting of the posterior covariance trace is penalized by a weighted norm of the state error sensitivities, and desensitized state estimates were obtained by minimizing this cost function. Then, the concept of the desensitized Kalman filter (DKF) was to extended to desensitized divided difference filtering [26] , desensitized unscented Kalman filtering [26], in which the cost function was augmented the same penalty function. The effectiveness of DKF was demonstrated by applications [19,26]. However, in the DKF the gain matrix is obtained by solving a linear equation, not a closed-form solution.

This paper presented a robust integrated navigation algorithm during the Mars atmospheric entry based on a special robust DEKF with analytical gain (ADEKF). The robust ADEKF is designed by minimizing a new cost function penalized by a trace weighted norm of the state error sensitivities, which has a scalar sensitivity-weight for each uncertain parameter, and obtaining a closed-form gain matrix. External IMU outputs and radio measurements between the vehicle and orbiting/surface beacons as observations are embedded into the navigation filter. In the above IMU/Radio beacons scheme, the uncertainties of the atmospheric density percentage and the LDR percentage are modeled, and the corresponding sensitivity matrices and perturbation matrices of the vehicle's state estimate errors are presented to describe the effect of the atmospheric density uncertainty and the LDR uncertainty. The robust ADEKF is introduced to overcome the negative

effects of initial state errors, atmospheric density uncertainty and LDR uncertainty during the Mars entry, and improves the entry integrated navigation robustness and accuracy.

The paper is organized as follows. Section 2 introduces the Mars entry dynamic model and models the atmospheric density uncertainty and the LDR uncertainty. Section 3 presents the special robust ADEKF based on the sensitivity matrix, and the corresponding perturbation matrix. Section 4 discusses the results of the numerical simulations and tests the covariance consistency of the filtering, based on the IMU/Radio measurement integrated navigation. The conclusions are summarized in Section 5.

2 Mars entry navigation dynamical system

To overcome the limited available navigation observable measurements during the Mars entry, recent research found that the ionizing plasma around the entry vehicle can be penetrated by the ultra-high frequency band radio communication [14,17]. A new auto-navigation scheme based on the orbiting/surface radio beacons (also called Mars network) is proposed to improve the observability and entry navigation accuracy for the future Mars landing missions.

Another problem is that the performance of an integrated navigation filter depends largely on the accuracy of the dynamic model. During the Mars entry phase, there are larger uncertainties in the vehicle aerodynamic characteristics, such as the LDR, and the atmospheric density. Unfortunately, it is difficult to precisely model the entry dynamic equations. The parameter uncertainties in the entry dynamic models must be considered. The three degree of freedom dynamic equations are defined in the subsequent section.

2.1 Dynamic model

For the sake of simplicity, the entry vehicle is assumed to fly in a stationary and quiet atmosphere of a non-rotating planet. The entry dynamic equations of the Mars entry vehicle in the Mars centered Mars-fixed coordinate system are given by[4,28]

$$\begin{aligned}
\dot{r} &= v \sin \gamma \\
\dot{v} &= -D - g(r) \sin \gamma \\
\dot{\gamma} &= \left(\frac{v}{r} - \frac{g(r)}{v} \right) \cos \gamma + \frac{L}{v} \cos \phi \\
\dot{\theta} &= \frac{v \cos \gamma \sin \psi}{r \cos \lambda} \\
\dot{\lambda} &= \frac{v \cos \gamma \cos \psi}{r} \\
\dot{\psi} &= \frac{v}{r} \sin \psi \cos \gamma \tan \lambda + \frac{L}{v \cos \gamma} \sin \phi
\end{aligned} \tag{1}$$

where the altitude r is the distance from center of the entry vehicle mass to center of the Mars; v is the radial velocity of the entry vehicle; γ is the flight path angle (FPA); θ is the longitude and λ is the latitude. The azimuth angle ψ is defined as a clockwise rotation angle starting at due north; and ϕ is the bank angle, which is fixed at zero in this work. The gravitational acceleration is $g(r) = \mu/r^2$ and μ is gravitational constant of the Mars. D and L are respectively the aerodynamic drag and lift accelerations given by

$$D = B\bar{q} \tag{2}$$

$$L = D \cdot L/D \tag{3}$$

where L/D is the LDR, $\bar{q} = \rho v^2 / 2$ is the dynamic pressure, and $B = C_D S / m$ is the ballistic coefficient, C_D is the vehicle drag coefficients, S represents the vehicle reference surface area, m denotes the mass of the vehicle, ρ denotes the Mars atmospheric density.

2.2 Measurement model

In this work, an integrated navigation scheme, in which there are one orbiting radio beacon and two predeployed surface radio beacons, is indicated to increase the observation information. The new observation information is the two-way range measurement, which is measured by the radio communication between the vehicle and a orbiting radio satellite or a surface radio beacon (such as the previous landers on the Mars) within sight[29]. The possible radio beacon sources for the Mars entry integrated navigation are shown in Fig. 1. Of course, the IMU will provide three components of acceleration and attitude rates during the Mars entry.

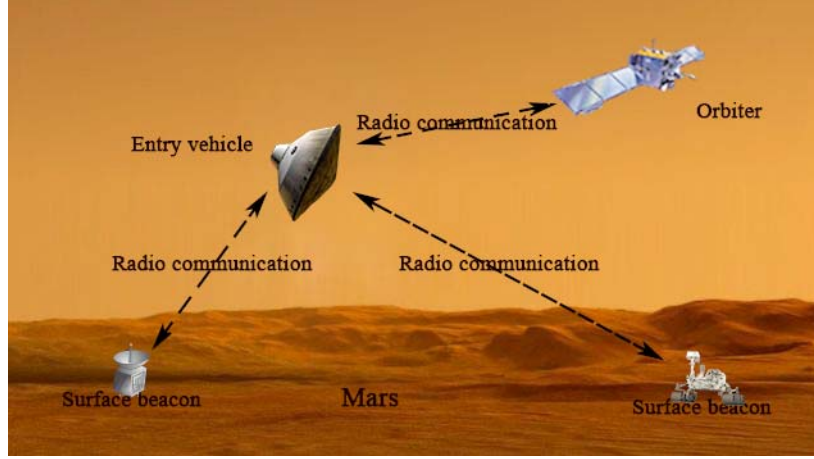


Fig.1 Diagram of IMU/Radio Measurement based on integrated navigation

2.2.1 IMU measurement

The accelerometers of the IMU measure the specific force components along three orthogonal axes. Three components of acceleration measured by the accelerometers are provided by

$$\tilde{\mathbf{a}} = \mathbf{a} + \mathbf{b}_a + \boldsymbol{\eta}_a \quad (4)$$

where $\tilde{\mathbf{a}}$ is the accelerometer output along body axes, \mathbf{a} is the true linear acceleration, \mathbf{b}_a is the acceleration bias, $\boldsymbol{\eta}_a$ is the zero-mean white Gaussian noise.

In this study, the accelerometer measurement model is defined as

$$\mathbf{a} = [-D \quad -D \cdot L/D \cdot \sin \phi \quad D \cdot L/D \cdot \cos \phi]^T \quad (5)$$

2.2.2 Two-way Range Measurement

The two-way range measurement provides the distance between the entry vehicle and an orbiting radio satellite or a surface radio beacon [29]. The two-way range measurement \tilde{R} is reconstructed by

$$\tilde{R}_k = \sqrt{(\mathbf{r}_l - \mathbf{r}_k)^T (\mathbf{r}_l - \mathbf{r}_k)} + \xi_R \quad (6)$$

where \mathbf{r}_l is the position vector of entry vehicle; \mathbf{r}_k is the position vector of orbiting radio satellite ($k = o$) or surface radio beacon ($k = b$); and ξ_R is the range noise with zero-mean Gaussian white noise.

2.3 Martian atmosphere uncertainty model

The Martian atmosphere model is very important for the Mars entry dynamic model, and directly affects the landing precision level of the vehicle. The Martian atmosphere model uncertainty mainly comes from the density, wind, dust content etc. The NASA Marshall Space Flight Center given a high-fidelity Mars-GRAM atmospheric model considering the variation of temperature, pressure, density and wind components with height, latitude, time of day and celestial longitude of the Sun [30]. The Committee on Space Research (COSPAR) established the COSPAR model of the Martian atmosphere, which based on the interpolation of the Viking data, and it is often used as a time invariant approximate atmospheric model in the filters. However, these models only can simple forecast the Martian atmosphere and density of the upper atmosphere, but inaccurately.

For the great uncertainty, the effect of the complex models is degraded. In fine, an approximate exponential Mars atmospheric density model in this work is assumed as follows

$$\rho = \rho_0 \exp\{(r_0 - r)/h_s\} \quad (7)$$

where ρ_0 denotes the nominal reference density on the surface of the Mars, r_0 is the nominal reference radial position ($r_0 = 3,437.2\text{km}$), and h_s is the constant scale height ($h_s = 7.5\text{km}$).

So the density uncertainty is described as

$$\rho_0 = \bar{\rho}_0 + c_1 \times \bar{\rho}_0 \quad (8)$$

where $\bar{\rho}_0$ is the nominal reference density, c_1 is the percentage of the atmosphere density uncertainty.

2.4 Lift-to-drag ratio uncertainty model

The LDR is very important for the choice of landing sites and the entry atmospheric zone of the vehicle from the orbit. The choice of landing sites is constrained to surface within a hundred kilometers by using a low LDR vehicle, and a high LDR vehicle can enlarge longitudinal and lateral ranges of the landing site and enhanced the mission flexibility [31].

The LDR is defined as the ratio of the lift coefficient C_L to the drag coefficient C_D , and its

general expression is

$$L / D = \frac{C_L}{C_D} \quad (9)$$

In general, C_L and C_D are not constant for the vehicle flight usually goes through both hypersonic and supersonic flight regimes. Design for simplicity, the aerodynamic coefficients C_L and C_D will be assumed to be constants in filtering implementation, although the LDR will be at its peak values during the dynamic part of the entry.

For the pinpoint landing mission, the LDR uncertainty should be considered, and the uncertainty propagation law should be researched. In fine, the percentage uncertainty of the LDR is modeled by

$$L / D = \overline{L / D_0} + c_2 \cdot \overline{L / D_0} \quad (10)$$

where $\overline{L / D_0}$ is the nominal reference LDR, c_2 is the percentage of the LDR uncertainty.

2.5 Mars entry navigation system

During the Mars entry phase, $\mathbf{x} = [r \ \theta \ \lambda \ v \ \gamma \ \psi]^T$ is defined as the state variables of the entry vehicle. The dynamic model in (1) is rewritten with the noise term $\mathbf{w}(t)$ as follows:

$$\dot{\mathbf{x}}(t) = \mathbf{f}(\mathbf{x}(t), \mathbf{c}, t) + \mathbf{w}(t) = \begin{bmatrix} v \sin \gamma \\ -D - g(r) \sin \gamma \\ \left(\frac{v}{r} - \frac{g(r)}{v} \right) \cos \gamma + \frac{L}{v} \cos \phi \\ \frac{v \cos \gamma \sin \psi}{r \cos \lambda} \\ \frac{v \cos \gamma \cos \psi}{r} \\ \frac{v}{r} \sin \psi \cos \gamma \tan \lambda + \frac{L}{v \cos \gamma} \sin \phi \end{bmatrix} + \mathbf{w}(t), \quad (11)$$

and the measurement model with noise $\mathbf{v}(t)$ is constructed by

$$\mathbf{z}(t) = \mathbf{h}(\mathbf{x}(t), \mathbf{c}, t) + \mathbf{v}(t) = \left[\mathbf{a} \ \tilde{R}_1 \ \tilde{R}_2 \ \tilde{R}_3 \right]^T \quad (12)$$

where \mathbf{c} denotes the uncertain parameter vector in the dynamic model, and $\tilde{R}_i (i=1,2,3)$ is the two-way range measurements.

In the subsequent integrated navigation the above dynamical models can be discretized as

follows

$$\mathbf{x}_k = \mathbf{f}(\mathbf{x}_{k-1}, \mathbf{c}, t_{k-1}) + \mathbf{w}_{k-1} \quad (13)$$

$$\mathbf{z}_k = \mathbf{h}(\mathbf{x}_k, \mathbf{c}, t_{k-1}) + \mathbf{v}_k \quad (14)$$

where \mathbf{w}_k and \mathbf{v}_k are independent zero-mean Gaussian noise processes, and their covariance are respectively \mathbf{Q}_k and \mathbf{R}_k . They satisfy

$$E[\mathbf{w}_k \mathbf{w}_j^T] = \mathbf{Q}_k \delta_{ij}, \quad E[\mathbf{v}_k \mathbf{v}_j^T] = \mathbf{R}_k \delta_{ij}, \quad E[\mathbf{w}_k \mathbf{v}_j^T] = \mathbf{0} \quad (15)$$

where δ_{ij} is the Kronecker delta function, and \mathbf{Q}_k is positive semi-definite, and \mathbf{R}_k is positive definite.

3 Robust desensitized extended Kalman filtering based on parameter sensitivity

Without loss of generality, consider the discrete nonlinear process and measurement models given by

$$\mathbf{x}_k = \mathbf{f}(\mathbf{x}_{k-1}, \mathbf{c}, \mathbf{w}_{k-1}, t_{k-1}) \quad (16)$$

$$\mathbf{z}_k = \mathbf{h}(\mathbf{x}_k, \mathbf{c}, \mathbf{v}_k, t_k) \quad (17)$$

where \mathbf{x}_k is the $n \times 1$ state vector, and \mathbf{z}_k is the $m \times 1$ measurement vector. \mathbf{f} is the dynamic vector-valued function, \mathbf{h} is the nonlinear measurement vector-valued function. \mathbf{c} is referred to as the $\ell \times 1$ uncertain parameter vector. \mathbf{w}_k and \mathbf{v}_k satisfy the conditions in (15).

In this work, the uncertain model parameter vector is assumed as a pre-estimate $\mathbf{c} = \hat{\mathbf{c}}$, with the a priori knowledge.

3.1 Extended Kalman filter

In the conventional extended Kalman filter, the state time update equations are

$$\hat{\mathbf{x}}_k^- = \mathbf{f}(\hat{\mathbf{x}}_{k-1}^+, \bar{\mathbf{c}}, 0, t_{k-1}) \quad (18)$$

$$\mathbf{P}_k^- = E[\mathbf{e}_k^- \mathbf{e}_k^{-T}] = \Phi_{k/k-1} \mathbf{P}_{k-1}^+ \Phi_{k/k-1}^T + \Gamma_{k-1} \mathbf{Q}_{k-1} \Gamma_{k-1}^T \quad (19)$$

where the superscripts $-$ denote a priori and $+$ denote a posteriori, and the overbar indicates the

corresponding estimate function of the parameter. $\Phi_{k/k-1} = \left. \frac{\partial \mathbf{f}(\mathbf{x}_{k-1}, \bar{\mathbf{c}}, \mathbf{w}_{k-1}, t_{k-1})}{\partial \mathbf{x}_{k-1}} \right|_{\mathbf{x}_{k-1} = \hat{\mathbf{x}}_{k-1}^+}$ and

$\Gamma_k = \left. \frac{\partial \mathbf{f}(\mathbf{x}_k, \bar{\mathbf{c}}, \mathbf{w}_k, t_k)}{\partial \mathbf{w}_k} \right|_{\mathbf{x}_k = \hat{\mathbf{x}}_k^+}$ are the coefficient matrices. \mathbf{P}_k^- is the error covariance propagation

matrix, and $\mathbf{e}_k^- = \hat{\mathbf{x}}_k^- - \mathbf{x}_k$ is the a priori estimation error.

The measurement update equations are

$$\hat{\mathbf{x}}_k^+ = \hat{\mathbf{x}}_k^- + \mathbf{K}_k [\mathbf{z}_k - \mathbf{h}(\hat{\mathbf{x}}_k^-, \bar{\mathbf{c}}, 0, t_k)] \quad (20)$$

$$\mathbf{P}_k^+ = E[\mathbf{e}_k^+ \mathbf{e}_k^{+T}] = (\mathbf{I} - \mathbf{K}_k \mathbf{H}_k) \mathbf{P}_k^- (\mathbf{I} - \mathbf{K}_k \mathbf{H}_k)^T + \mathbf{K}_k \Upsilon_k \mathbf{R}_k \Upsilon_k^T \mathbf{K}_k^T \quad (21)$$

$$\mathbf{K}_k = \mathbf{P}_k^- \mathbf{H}_k^T (\mathbf{H}_k \mathbf{P}_k^- \mathbf{H}_k^T + \Upsilon_k \mathbf{R}_k \Upsilon_k^T)^{-1} \quad (22)$$

where $\mathbf{H}_k = \left. \frac{\partial \mathbf{h}(\mathbf{x}_k, \bar{\mathbf{c}}, \mathbf{v}_k, t_k)}{\partial \mathbf{x}_k} \right|_{\mathbf{x}_k = \hat{\mathbf{x}}_k^-}$ and $\Upsilon_k = \left. \frac{\partial \mathbf{h}(\mathbf{x}_k, \bar{\mathbf{c}}, \mathbf{v}_k, t_k)}{\partial \mathbf{v}_k} \right|_{\mathbf{x}_k = \hat{\mathbf{x}}_k^-}$ are the coefficient matrices. \mathbf{P}_k^+ is

the state estimate error covariance matrix, and $\mathbf{e}_k^+ = \hat{\mathbf{x}}_k^+ - \mathbf{x}_k$ is the a posteriori estimation error. (21)

is valid for any \mathbf{K}_k . The Kalman optimal gain \mathbf{K}_k is obtained by minimizing the cost function

$J = \text{Tr}(\mathbf{P}_k^+)$, in which “Tr” denotes the trace of the matrix, and the result is (22).

Under the basic assumptions of the Kalman filter (no model and parameter uncertainty, zero-mean white-noise sequence, known process and measurement models, etc.), the state estimate are unbiased. It means that the estimation errors of the Kalman filter satisfy

$$E[\mathbf{e}_k^-] = 0, E[\mathbf{e}_k^+] = 0 \quad (23)$$

3.2 Sensitivity matrix and perturbation matrix

For the model parameter uncertainties, the basic assumptions of the Kalman filter cannot be

satisfied, and the state estimates may be biased and even divergence. So, the state estimate error sensitivities of the parameter vector \mathbf{c} could be defined as [27,32]

$$\mathbf{S}_k^- = \frac{\partial \mathbf{e}_k^-}{\partial \mathbf{c}} = \frac{\partial \hat{\mathbf{x}}_k^-}{\partial \mathbf{c}} \quad (24)$$

$$\mathbf{S}_k^+ = \frac{\partial \mathbf{e}_k^+}{\partial \mathbf{c}} = \frac{\partial \hat{\mathbf{x}}_k^+}{\partial \mathbf{c}} \quad (25)$$

where $\mathbf{S} = (\mathbf{s}_1, \mathbf{s}_2, \dots, \mathbf{s}_\ell)$ is the $n \times \ell$ sensitivity matrix, $\mathbf{s}_i = \partial \hat{\mathbf{x}} / \partial c_i$ denotes the sensitivities of the state estimate $\hat{\mathbf{x}}$ to the i th component of the parameter vector \mathbf{c} . Note that the sensitivity of the true state is $\partial \mathbf{x} / \partial \mathbf{c} = 0$ in (24) and (25) because the true state doesn't vary with the assumed value of parameter vector \mathbf{c} .

From the basic equations (18) and (20) of the conventional Kalman filter, the propagation equations can be obtain by

$$\mathbf{S}_k^- = \Phi_{k/k-1} \mathbf{S}_{k-1}^+ + \Psi_{k-1} \quad (26)$$

$$\mathbf{S}_k^+ = \mathbf{S}_k^- - \mathbf{K}_k \gamma_k \quad (27)$$

where $\Psi_{k-1} = \left. \frac{\partial f(\hat{\mathbf{x}}_{k-1}^+, \mathbf{c}, \mathbf{w}_{k-1}, t_{k-1})}{\partial \mathbf{c}} \right|_{\mathbf{c}=\bar{\mathbf{c}}}$, and

$$\gamma_k = \mathbf{H}_k \mathbf{S}_k^- + \mathbf{H}_k^c \quad (28)$$

where $\mathbf{H}_k^c = \left. \frac{\partial \mathbf{h}(\hat{\mathbf{x}}_k^-, \mathbf{c}, \mathbf{v}_k, t_k)}{\partial \mathbf{c}} \right|_{\mathbf{c}=\bar{\mathbf{c}}}$. Note that the sensitivity of gain matrix is assumed as $\partial \mathbf{K} / \partial \mathbf{c} = 0$ in

(27), because any $\partial \mathbf{K} / \partial \mathbf{c} \neq 0$ means that the solution for the optimal gain is a function of the residual, which violates the basis for the linear update equation given in (20) [24,27].

The sensitivity matrix describes how the state estimate $\hat{\mathbf{x}}$ varies with the uncertain parameter vector \mathbf{c} . To evaluate the effect of the parameter uncertainties to the state estimate error, the perturbation matrix is defined by

$$\mathbf{\Gamma} = \mathbf{S} \cdot \Sigma_c \quad (29)$$

where $\Sigma_c = \text{diag}[\sigma_{c_1}, \sigma_{c_2}, \dots, \sigma_{c_\ell}]$ denotes the diagonal matrix, in which the elements are the standard deviation σ_{c_i} ($i=1, 2, \dots, \ell$) of each parameter. Each element, Γ_{ij} , of the perturbation matrix Γ gives the error in the state estimate $\hat{\mathbf{x}}$ due to 1σ error in each uncertain parameter c_j .

3.3 Robust desensitized extended Kalman filtering with analytical gain

To solve the negative effects of the parameter uncertainties, Karlgaard and Shen [24-25] introduced the desensitized optimal control methodology into the filtering, and proposed a desensitized optimal filtering to mitigate these negative effects based on a new cost function including the state error sensitivities. They defined the state error sensitivities $\mathbf{s}_{i,k}^- = \partial \hat{\mathbf{x}}_k^- / \partial c_i$ and $\mathbf{s}_{i,k}^+ = \partial \hat{\mathbf{x}}_k^+ / \partial c_i$ to each parameter c_i , and augmented the cost function consisting of the posterior covariance trace with a penalty function consisting of a weight normal of the a posterior sensitivity by

$$J = \text{Tr}(\mathbf{P}_k^+) + \sum_{i=1}^{\ell} \mathbf{s}_{i,k}^{+T} \mathbf{W}_i \mathbf{s}_{i,k}^+ \quad (30)$$

where \mathbf{W}_i is a $n \times n$ user-specified symmetric positive semi-definite sensitivity-weighting matrix for the i th sensitivity. Here, the sensitivity-weighting matrix \mathbf{W}_i is a time-variant tuning parameter, which makes a balance between the possibly competing objectives of minimizing the variance and minimizing the sensitivity.

Then, taking the derivative with respect to \mathbf{K}_k , and setting $\partial J / \partial \mathbf{K}_k = 0$, yields a linear matrix equation about the gain matrix \mathbf{K}_k

$$\mathbf{K}_k (\mathbf{H}_k \mathbf{P}_k^- \mathbf{H}_k^T + \Upsilon_k \mathbf{R}_k \Upsilon_k^T) + \sum_{i=1}^{\ell} \mathbf{W}_i \mathbf{K}_k \boldsymbol{\gamma}_{i,k} \boldsymbol{\gamma}_{i,k}^T = \mathbf{P}_k^- \mathbf{H}_k^T + \sum_{i=1}^{\ell} \mathbf{W}_i \mathbf{s}_{i,k}^- \boldsymbol{\gamma}_{i,k}^T, \quad (31)$$

and solving algebraically the linear equation will obtain the gain matrix \mathbf{K}_k . This implies that the cost of the computational power and the processing time required will increase rapidly, especially

when the dimension of the state is large.

In this work, based on the sensitivity matrices in (26) and (27), which are different from the definitions in DEKF, a special robust desensitized extended Kalman filter with analytical gain is presented. This special case of the DEKF simplifies the sensitivity-weighting matrix of the uncertain parameters by substituting the $n \times n$ matrix \mathbf{W}_i for a scalar, and this makes that the gain matrix obtained by solving a linear matrix equation is instead of a closed-form solution.

A new cost function based on the posterior covariance trace and a trace penalty function consisting of the weighted norm of the posterior sensitivity matrix is redefined as

$$J_a = Tr(\mathbf{P}_k^+) + Tr(\mathbf{S}_k^+ \mathbf{W} \mathbf{S}_k^{+T}) \quad (32)$$

where \mathbf{W} is a $\ell \times \ell$ symmetric positive semi-definite weighting matrix for the uncertain parameters. This sensitivity-weighting matrix is a diagonal matrix, in which each element on the main diagonal is the scalar sensitivity-weighting of each uncertain parameter for all the states of the dynamic model.

Substituting (21) and (27) into (32) and taking the derivative with respect to the gain \mathbf{K}_k , and using the trace derivative properties in Appendix A, yields

$$\begin{aligned} \frac{\partial J_a}{\partial \mathbf{K}_k} &= \frac{\partial}{\partial \mathbf{K}_k} Tr(\mathbf{P}_k^+) + \frac{\partial}{\partial \mathbf{K}_k} Tr(\mathbf{S}_k^+ \mathbf{W} \mathbf{S}_k^{+T}) \\ &= 2\mathbf{K}_k (\mathbf{H}_k \mathbf{P}_k^- \mathbf{H}_k^T + \Upsilon_k \mathbf{R}_k \Upsilon_k^T) - 2\mathbf{P}_k^- \mathbf{H}_k^T - 2\mathbf{S}_k^- \mathbf{W} \boldsymbol{\gamma}_k^T + 2\mathbf{K}_k \boldsymbol{\gamma}_k \mathbf{W} \boldsymbol{\gamma}_k^T \end{aligned} \quad (33)$$

Setting $\partial J / \partial \mathbf{K}_k = 0$ and simplifying the formulation, the analytical gain matrix is given as follows

$$\mathbf{K}_k = (\mathbf{P}_k^- \mathbf{H}_k^T + \mathbf{S}_k^- \mathbf{W} \boldsymbol{\gamma}_k^T) (\mathbf{H}_k \mathbf{P}_k^- \mathbf{H}_k^T + \boldsymbol{\gamma}_k \mathbf{W} \boldsymbol{\gamma}_k^T + \Upsilon_k \mathbf{R}_k \Upsilon_k^T)^{-1} \quad (34)$$

Remark: The formulation of the gain \mathbf{K}_k in (34) is similar in a well-known form to the conventional Kalman filter and it is a closed-form solution, too.

4 Simulation Results and Analysis

MATLAB / Simulink simulations under the IMU/Radio communication integrated navigation scheme during the Mars entry phase have been carried out to show that the sensitivities of the state estimate errors respected to the uncertain parameter, the perturbations coming from the parameter uncertainty, and the performance of the proposed robust ADEKF.

The simulation conditions and parameters, in which the truth and the initial values are all listed, are summarized in Table 1[33]. The initial position of orbiting beacon is (7,855,700m, -461,800m, 749,820m) , and the corresponding constant velocity is (66.2 m/s, 2,206.4 m/s, -413 m/s). The positions of two surface beacons are (3,300,000m, 420,000m, 1,350,000m) and (3,290,000m, 570,000m, 755,000m), respectively, and their velocities are assumed to zeros.

Table 1 Initial conditions and model parameters for integrated navigation

| Parameters | True | Estimated/Initial |
|----------------------------|---------------------------|----------------------------|
| Initial altitude r | 3518.2km | 3519.2km |
| Initial velocity v | 5515 m/s | 5525m/s |
| Initial FPA γ | -11.8deg | -12deg |
| Initial longitude θ | -89.872deg | -90.072deg |
| Initial latitude λ | -28.02deg | -28.22deg |
| Initial azimuth ψ | 5.156deg | 5.356deg |
| Ballistic coefficient B | 0.016 m ² / kg | 0.0176 m ² / kg |

The gravitational constant of the Mars is $\mu=42,828.29 \times 10^9 \text{ m}^3/\text{s}^2$. The acceleration bias of IMU is -0.03 m/s^2 . The nominal reference atmospheric density is $\bar{\rho}_0=2.0 \times 10^{-4} \text{ kg/m}^3$ and the nominal reference LDR is $\bar{L}/D_0=0.156$. The true percentage of the atmospheric density uncertainty and the LDR uncertainty are assumed to be unknown, which are assumed to subject to uniform distributions in simulations, that are respectively $c_1 \sim U(-0.15, 0.15)$ and $c_2 \sim U(-0.1, 0.1)$; and in the model they are assumed that $c_1 = 0$ and $c_2 = 0$. The sensitivity-weighting matrix in the proposed robust ADEKF is given by $W = \text{diag}[0.01, 0.1]$. In the IMU/Radio communication integrated navigation scheme, three possible beacons are selected to provide the two-way range

measurements. Initial state error covariance matrix is $\mathbf{P}_0 = \text{diag}[10^6, 10^5, 10^{-1}, 10^{-5}, 10^{-5}, 10^{-1}]$, process noise covariance matrix is $\mathbf{Q}_k = \text{diag}[10, 1, 10^{-6}, 10^{-10}, 10^{-10}, 10^{-6}]$, and measurement noise covariance matrix is $\mathbf{R}_k = \text{diag}[10^{-6}, 10^{-6}, 10^{-6}, 20, 20, 40]$.

The simulation is terminated roughly after 400s when the supersonic chute is deployed. 5,000 simulations have run, the root mean squared error (RMSE) is averaged, and the covariance consistency is testing by the normalized mean error (NME) test [34]. In the simulation, we selected the EKF as the comparing filtering.

Figure 2 shows the sensitivities of the six navigation state estimate errors of the EKF and the ADEKF respected to the percentage of the atmospheric density uncertainty when $c_1 = 7.5\%$ and $W = \text{diag}[0.01, 0]$; Fig. 3 shows the sensitivities of the six navigation state estimate errors of the EKF and the ADEKF respected to the percentage of the LDR uncertainty when $c_2 = 5\%$ and $W = \text{diag}[0, 0.1]$; and Fig. 4 shows that the above state estimate error values of the ADEKF respected to the two uncertain parameters due to one-sigma errors in their uncertainty when $c_1 = 7.5\%$, $c_2 = -5\%$ and $W = \text{diag}[0.01, 0.1]$. In fact, the sensitivity respected to the uncertainty c_1 and c_2 represents the sensitivity respected to the atmospheric density and the LDR uncertainty, respectively. In Figs. 2 and 3, subfigures show the sensitivity of the ADEKF respected to the two uncertain parameters. In Fig. 2, it shows that the altitude, velocity, and FPA estimate errors in EKF filtering have great sensitivities respected to the atmospheric density uncertainty than these in ADEKF filtering. In Fig. 3, it can be seen that the longitude and latitude estimate errors have low sensitivities respected to the LDR uncertainty, and the others estimate errors are sensitive to the LDR uncertainty. Obviously, the ADEKF respected to the LDR uncertainty has lower sensitivities than those of the EKF in Figs. 2 and 3. The six state estimate perturbation errors coming from the one-sigma errors of the two uncertain parameters are shown in Fig. 4. From Fig.4, It can be seen that the state estimate perturbation errors coming from the atmospheric density are greater than the errors coming from the LDR after 40s during Mars entry. It implies that the negative effects of the atmospheric density uncertainty are greater than the LDR uncertainty. The EKF error accumulations of each step lead to gradually diverge, and the ADEKF effectively desensitize

the negative effects of the parameter uncertainties.

Figure 5 shows the results coming from a single run of the Monte Carlo simulations, which are the state estimate errors and 3σ bounds of ADEKF, when $c_1 = 7.5\%$, $c_2 = -5\%$ and $W = \text{diag}[0.01, 0.1]$. All the six state errors of the ADEKF are captured by the three-sigma covariance bounds for the most parts, and the filter slightly diverges for the FPA and azimuth. Fig.6 shows that the state estimate RMSEs of the EKF and the ADEKF with logarithmic scales. From Fig. 6, it can be seen that the RMSEs of the ADEKF are all obviously smaller than these of the EKF except the altitude, and in altitude slightly smaller than these of the EKF.

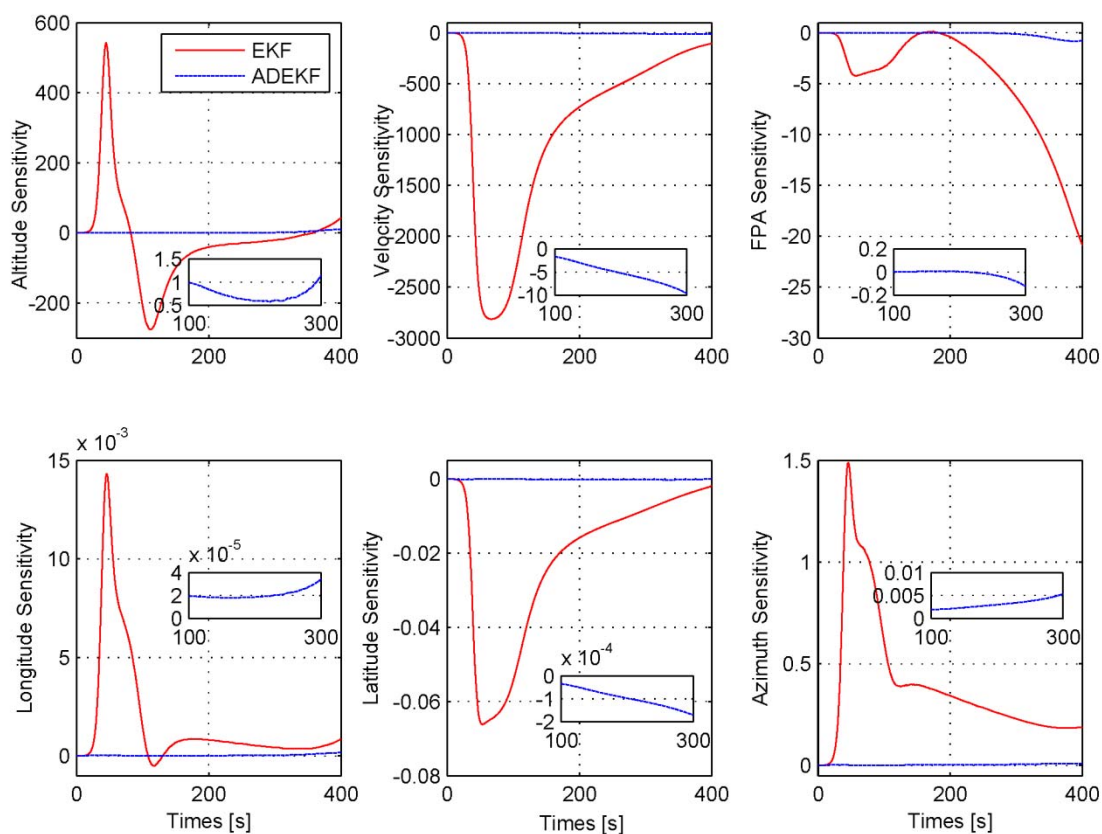


Fig.2 State Sensitivities of EKF and ADEKF respected to the atmospheric density ($c_1 = 7.5\%$, $c_2 = 0$)

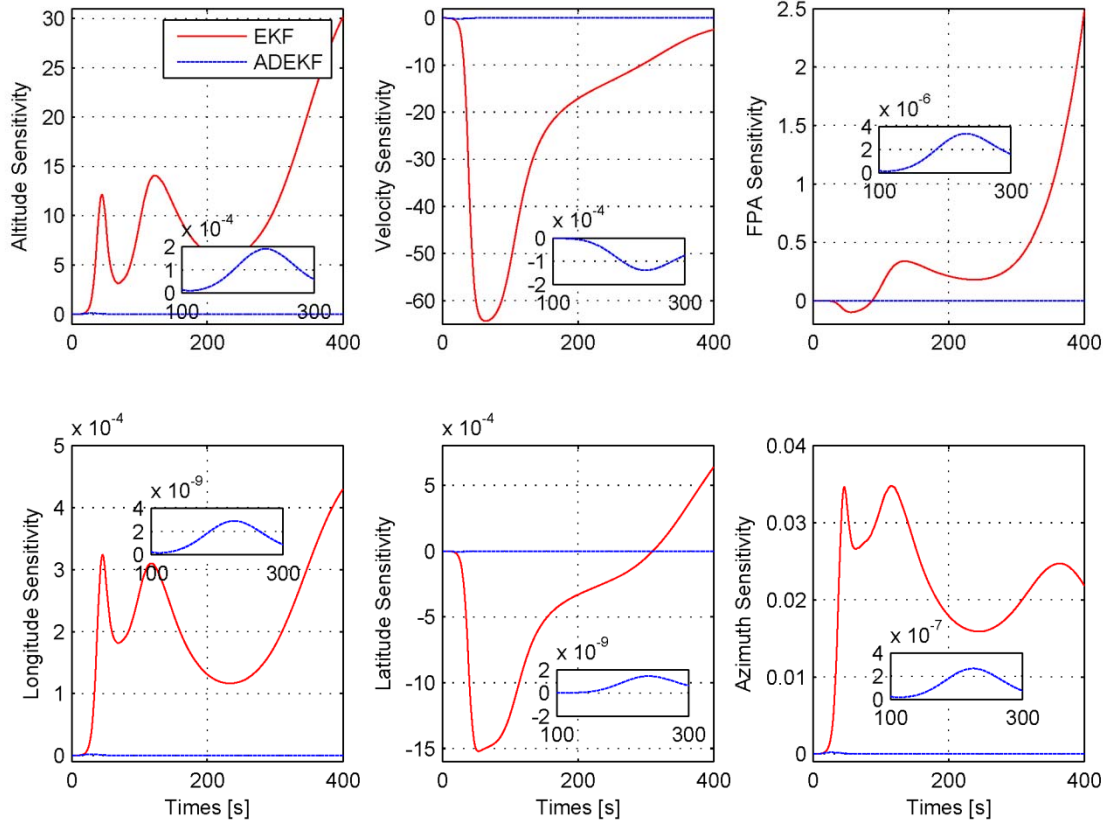


Fig.3 State Sensitivities of EKF and ADEKF respected to the LDR ($c_1 = 0, c_2 = 5\%$)

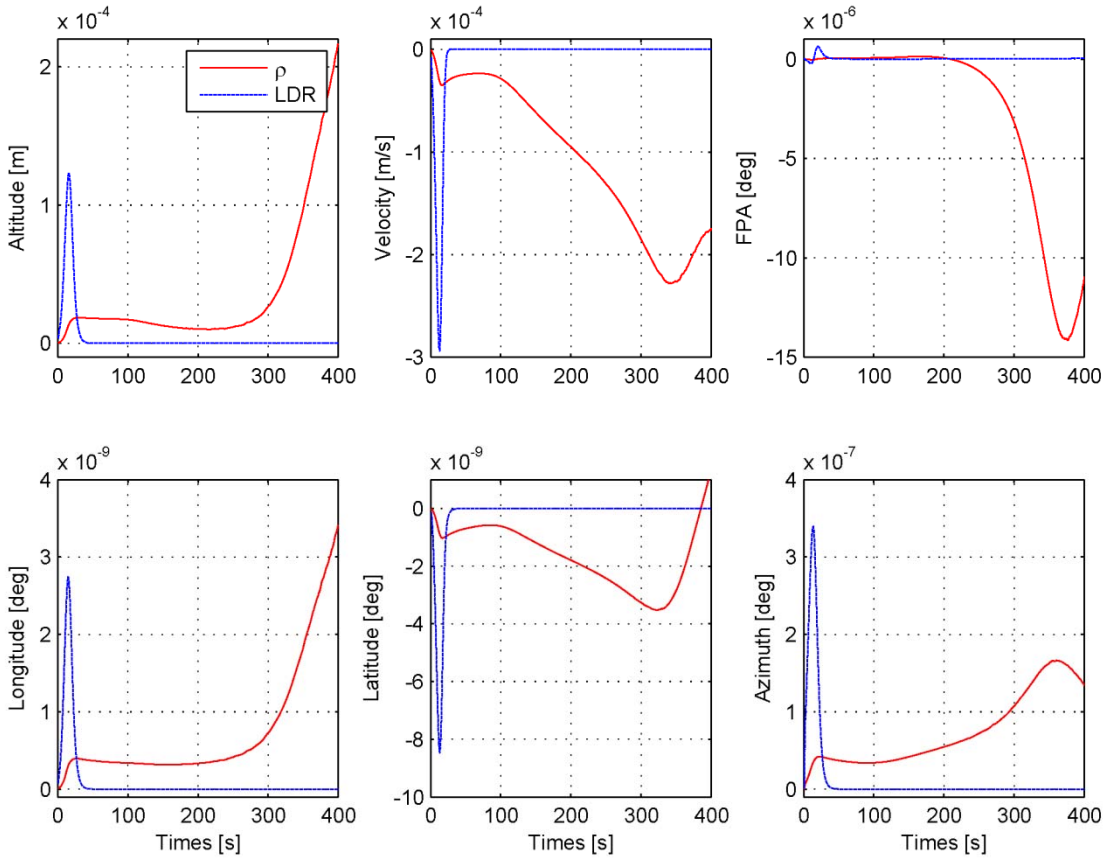


Fig.4 State estimate errors of ADEKF for 1σ error of the two parameters ($c_1 = 7.5\%, c_2 = -5\%$)

A filter consistency test is used to highlight the effectiveness of the covariance estimates in accounting for errors in the state estimates [34]. The results of the NME test with logarithmic scales are shown in Fig. 7. The ADEKF covariance estimate accurately predicts the state estimate errors, because all of its state test statistics are well below the required threshold. Obviously, the EKF results imply that it has poor consistency in the altitude, velocity, FPA, longitude and azimuth. It is to say that the ADEKF consistently provide excellent state estimate and the EKF has trouble accounting for the errors in the two uncertain parameters.

As a whole, the ADEKF effectively provides a large reduction in sensitivity respected to the two parameter uncertainties, enhances the robustness of integrated navigation, and improve the navigation accuracy.

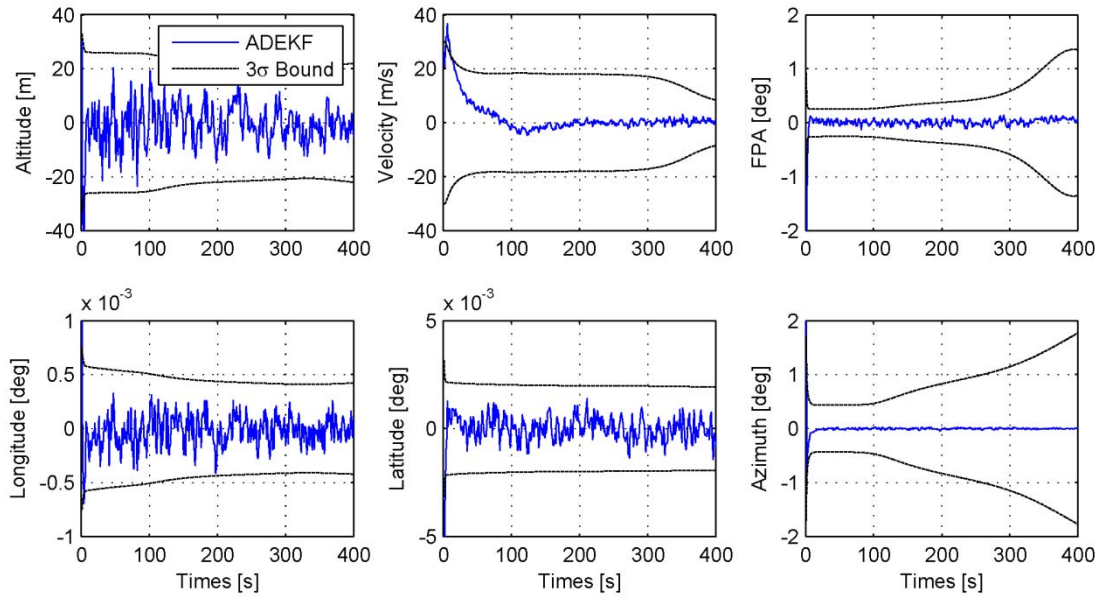


Fig.5 State estimate errors and 3σ bounds of ADEKF ($c_1 = 7.5\%, c_2 = -5\%$)

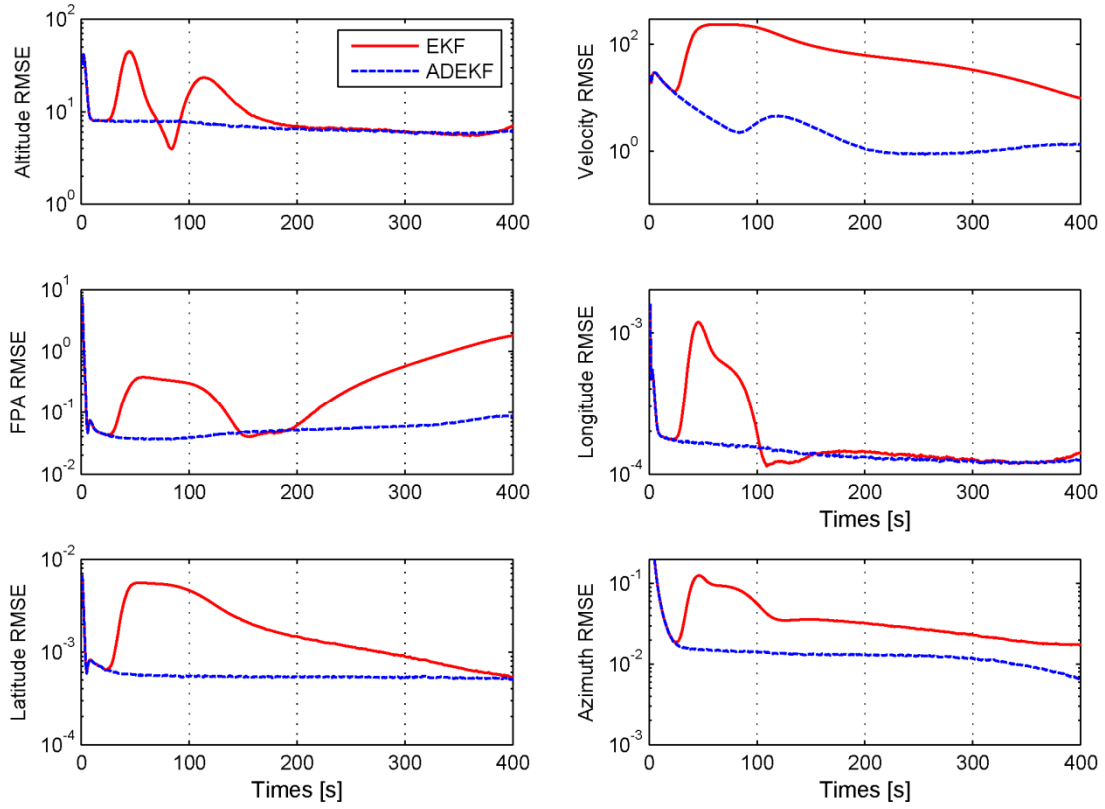


Fig.6 State estimate RMS errors of the EKF and ADEKF

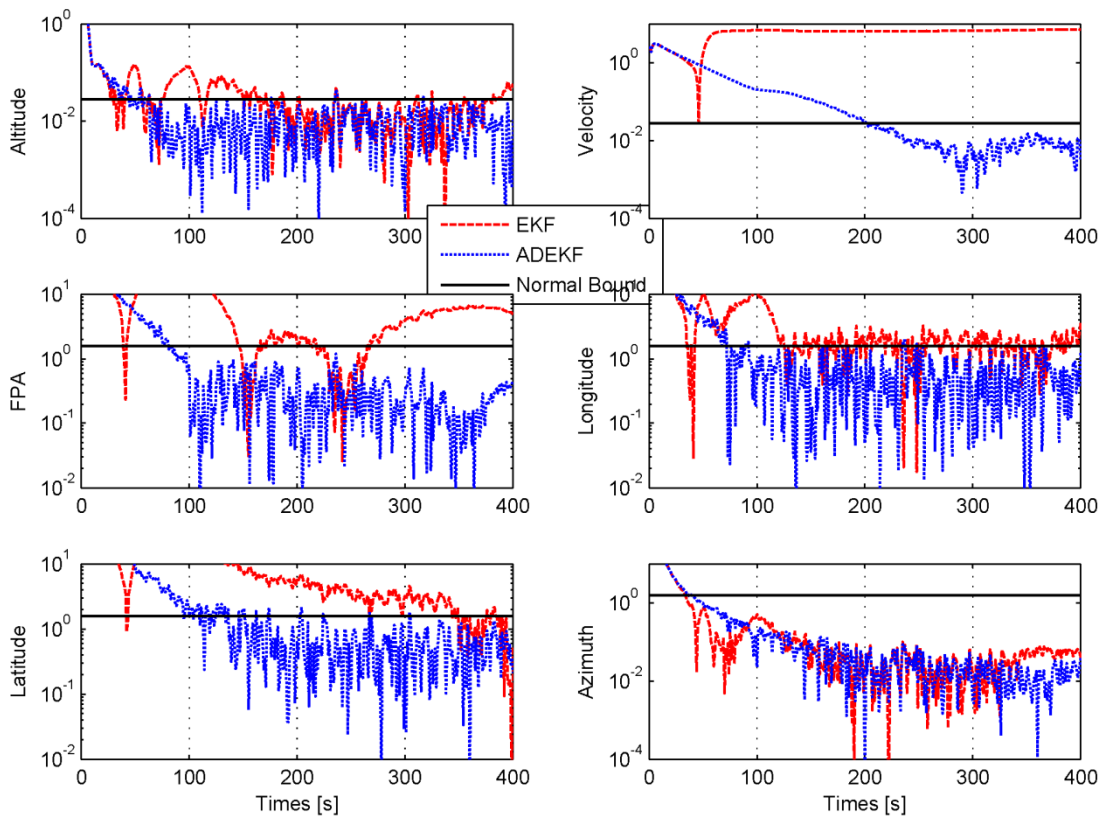


Fig.7 NME test results for state estimate errors

5 Conclusions

High-precision robust atmospheric entry navigation is a key technology to meet the future Mars exploration missions required the pinpoint landing capability. This paper presented a robust integrated navigation algorithm during the Mars atmospheric entry based on a special robust ADEKF. A new cost function penalized by a trace weighted norm of the state error sensitivities is minimized to give a closed-form gain matrix. In the IMU/Radio beacons scheme, the uncertainties of the atmospheric density and the LDR percentage are modeled, and the corresponding sensitivity matrices and perturbation matrices of the vehicle's state estimate errors are proposed to describe the effect of their uncertainties. Numerical simulations and the consistency test show that the robust integrated navigation algorithm based on the robust ADEKF effectively reduces the negative effects of the two parameter uncertainties during the Mars entry, and improves the entry navigation robustness and accuracy.

In this work, we give a special sensitivity-weighting matrix in the application during Mars entry. But, how to select and obtain the sensitivity-weighting matrix is an open problem. In the future work, we will focus on how to select a reasonable sensitivity-weighting matrix, which is beyond the scope of the present paper.

Appendix A- Matrix Trace Calculus

To get the optimal gain from the cost function in Kalman filter derivations, taking the partial derivative of the trace of matrix is often used. The corresponding results about the derivatives are

$$\frac{\partial}{\partial \mathbf{K}} Tr(\mathbf{K}\mathbf{P}) = \mathbf{P}^T \quad (\text{A.1})$$

$$\frac{\partial}{\partial \mathbf{K}} Tr(\mathbf{P}\mathbf{K}^T) = \mathbf{P} \quad (\text{A.2})$$

$$\frac{\partial}{\partial \mathbf{K}} Tr(\mathbf{K}\mathbf{P}\mathbf{K}^T) = \mathbf{K}\mathbf{P}^T + \mathbf{K}\mathbf{P} \quad (\text{A.3})$$

Where \mathbf{K} and \mathbf{P} are two arbitrary matrices satisfying matrix multiplication rules.

For the product of a column n-vector \mathbf{x} with itself, the traces of them satisfy

$$Tr(\mathbf{x}\mathbf{x}^T) = \mathbf{x}^T \mathbf{x} \quad (\text{A.4})$$

References

- [1] G.F. Mendeck, L.C. McGrew, Post-Flight EDL Entry Guidance Performance of the 2011 Mars Science Laboratory Mission, in: 2013 AAS/AIAA Spaceflight Mechanics, Kauai, HI,US, 2013.
- [2] G. Wells, J. Lafleur, A. Verges, K. Manyapu, J. Christian, C. Lewis, R. Braun, Entry, Descent and Landing Challenges of Human Mars Exploration, in: 29th annual AAS Guidance and Control Conference, Breckenridge, Colorado, 2006, 325.
- [3] S. Li, X.Q. Jiang, Review and prospect of guidance and control for Mars atmospheric entry, Prog Aerosp Sci. 69(2014) 40-57.
- [4] J.F. Levesque, J. de Lafontaine, Innovative navigation schemes for state and parameter estimation during mars entry, Journal of guidance, control, and dynamics. 30(2007) 169-184.
- [5] R.D. Braun, R.M. Manning, Mars exploration entry, descent, and landing challenges, J Spacecraft Rockets. 44(2007) 310-323.
- [6] C.C. Chu, Development of advanced entry, descent, and landing technologies for future Mars missions, in: 2006 IEEE Aerospace Conference, Big Sky, MT, 2006.
- [7] T.J. Martin-Mur, G.L. Kruizingas, P.D. Burkhart, M.C. Wong, F. Abilleira, Mars Science Laboratory Navigation Results, in: 23rd International Symposium on Space Flight Dynamics, Pasadena, California, 2012.
- [8] P.Y. Cui, Z.S. Yu, S.Y. Zhu, Research progress and prospect of autonomous navigation techniques for Mars entry phase, Journal of Astronautics. 34(2013) 447-456.
- [9] M.C. Heyne, R.H. Bishop, Spacecraft entry navigation using sigma point Kalman filtering, in: Proceedings of the IEEE/ION Position, Location and Navigation Symposium, San Diego, California, 2006, 71-79.
- [10] T.A. Ely, R.H. Bishop, O. Dubois-Matra, Robust entry navigation using hierarchical filter architectures regulated with gating networks, in: 16th International Symposium on Spaceflight Dynamics Symposium, Pasadena, CA, 2001.
- [11] R. Zanetti, R.H. Bishop, Adaptive Entry Navigation Using Inertial Measurements, in: 17th Annual Space Flight Mechanics Meeting, Sedona, AZ, 2007, 457-469.
- [12] P. Pastor, R.H. Bishop, S. Striepe, Evaluation of Mars Entry Reconstructed Trajectories Based on Hypothetical ‘Quick-Look’ Entry Navigation Data, in: AAS Paper 00-197, AAS/AIAA Space Flight Mechanics Meeting, Clearwater, Florida, 2000, 23-26.
- [13] R.C. Blanchard, R.H. Tolson, R.A. Lugo, L. Huh, Inertial Navigation Entry, Descent, and Landing Reconstruction Using Monte Carlo Techniques, in: Proceedings of the 23rd AAS/AIAA Space Flight Mechanics Meeting, Kauai, Hawaii, 2013.
- [14] D.D. Morabito, The spacecraft communications blackout problem encountered during passage or entry of planetary atmospheres, IPN Progress Report(2002) 42-150.
- [15] D.D. Morabito, K.T. Edquist, Communications blackout predictions for atmospheric entry of Mars Science Laboratory, in: 2005 IEEE Aerospace Conference, Big Sky, MT, 2005, 489-500.
- [16] E.G. Lightsey, A.E. Mogensen, P.D. Burkhart, T.A. Ely, C. Duncan, Real-time navigation for mars missions using the mars network, J Spacecraft Rockets. 45(2008) 519-533.
- [17] J.L. Williams, P.R. Menon, S.W. Demcak, Mars Reconnaissance Orbiter Navigation Strategy for Mars Science Laboratory Entry, Descent and Landing Telecommunication Relay Support, in:

- AIAA/AAS Astrodynamics Specialist Conference, Minneapolis, Minnesota, 2012.
- [18] S. Li, Y.M. Peng, Radio beacons/IMU integrated navigation for Mars entry, *Adv Space Res.* 47(2011) 1265-1279.
- [19] S. Li, X.Q. Jiang, Y.F. Liu, High-precision Mars entry integrated navigation under large uncertainties, *J Navigation.* 67(2014) 327-342.
- [20] B.A. Steinfeldt, M.J. Grant, D.A. Matz, R.D. Braun, G.H. Barton, Guidance, Navigation, and Control System Performance Trades for Mars Pinpoint Landing, *J Spacecraft Rockets.* 47(2010) 188 - 198.
- [21] H. Seywald, R.R. Kumar, Desensitized optimal trajectories, *Adv.Astronaut. Sci.*(1996) 103-116.
- [22] H.J. Shen, H. Seywald, R. Powell, Desensitizing the Pin-Point Landing Trajectory on Mars, in: AIAA/AAS Astrodynamics Specialist Conference and Exhibit, Honolulu, Hawaii, 2008.
- [23] H. Shen, H. Seywald, R.W. Powell, Desensitizing the minimum-fuel powered descent for Mars pinpoint landing, *Journal of guidance, control, and dynamics.* 33(2010) 108-115.
- [24] C.D. Karlgaard, H.J. Shen, Desensitized optimal filtering, in: AIAA Guidance, Navigation, and Control Conference, Portland, Oregon, 2011.
- [25] C.D. Karlgaard, H.J. Shen, Desensitized Kalman filtering, *IET Radar, Sonar & Navigation.* 7(2013) 2-9.
- [26] C.D. Karlgaard, H.J. Shen, Desensitized divided difference filtering for induction motor state estimation(2012) 145-150.
- [27] H.J. Shen, C.D. Karlgaard, Desensitized unscented Kalman Filter about uncertain model parameters, in: Institute of Navigation International Technical Meeting, Newport Beach, California, 2012.
- [28] M.K. Lockwood, R.W. Powell, C. Graves, Entry system design considerations for mars landers, in: AAS Guidance and Control Conference, Breckenridge, CO, 2001.
- [29] R.A. Boehmer, Navigation analysis and design for Mars entry. Massachusetts: Massachusetts Institute of Technology, 1999.
- [30] C.G. Justus, A. Duvall, V.W. Keller, Validation of Mars Global Reference Atmospheric Model (Mars-GRAM 2001) and planned new features, *Adv Space Res.* 38(2006) 2633-2638.
- [31] M.E. Tauber, J.V. Bowles, L. Yang, Atmospheric environment during maneuvering descent from Martian orbit, *J Spacecraft Rockets.* 26(1989) 330-337.
- [32] B.D. Tapley, B.E. Schutz, G.H. Born, Statistical orbit determination., Academic Press, New York, 2004.
- [33] Z. Yu, P. Cui, S. Zhu, Observability-based Beacon Configuration Optimization for Mars Entry Navigation, *Journal of Guidance, Control, and Dynamics*(2015) In press.
- [34] D. Woodbury, J. Junkins, On the Consider Kalman Filter, in: Proceedings of the AIAA Guidance, Navigation, and Control Conference, Toronto, Canada, 2010.